Published in final edited form as:
Gynecol Oncol. 2008 July ; 110(1): 99–109. doi:10.1016/j.ygyno.2008.03.006.

Ovarian normal and tumor-associated fibroblasts retain *in vivo* stromal characteristics in a 3-D matrix-dependent manner

Roderick M. Quiros[1,2,3], **Matthildi Valianou**[1,2], **Youngjoo Kwon**[3], **Kimberly M. Brown**[2,3], **Andrew K. Godwin**[3], and **Edna Cukierman**[2,4]

2*Basic Science, Fox Chase Cancer Center, Philadelphia, PA.*

3*Medical Science Divisions, Fox Chase Cancer Center, Philadelphia, PA.*

Abstract

Objective—Due to a lack of experimental systems, little is known about ovarian stroma. Here, we introduce an *in vivo*-like 3-D system of mesenchymal stromal progression during ovarian tumorigenesis to support the study of stroma permissiveness in human ovarian neoplasias.

Methods—To sort 3-D cultures into 'normal,' 'primed' and 'activated' stromagenic stages, 29 fibroblastic cell lines from 5 ovarian tumor samples (tumor ovarian fibroblasts, TOFs) and 14 cell lines from normal prophylactic oophorectomy samples (normal ovarian fibroblasts, NOFs) were harvested and characterized for their morphological, biochemical and 3-D culture features.

Results—Under 2-D conditions, cells displayed three distinct morphologies: spread, spindle, and intermediate. We found that spread and spindle cells have similar levels of α-SMA, a desmoplastic marker, and consistent ratios of pFAKY^{397}/totalFAK. In 3-D intermediate cultures, α-SMA levels were virtually undetectable while pFAKY^{397}/totalFAK ratios were low. In addition, we used confocal microscopy to assess *in vivo*-like extracellular matrix topography, nuclei morphology and α-SMA features in the 3-D cultures. We found that all NOFs presented 'normal' characteristics, while TOFs presented both 'primed' and 'activated' features. Moreover, immunohistochemistry analyses confirmed that the 3-D matrix-dependent characteristics are reminiscent of those observed in *in vivo* stromal counterparts.

Conclusions—We conclude that primary human ovarian fibroblasts maintain *in vivo*-like (staged) stromal characteristics in a 3-D matrix dependent manner. Therefore, our stromal 3-D system offers a tool that can enhance the understanding of both stromal progression and stroma-induced ovarian tumorigenesis. In the future, this system could also be used to develop ovarian stroma-targeted therapies.

Keywords

Extracellular matrix; 3-D culture; tumor stroma; tumor-associated fibroblasts

4Corresponding author: Edna Cukierman, PhD Basic Science Division Fox Chase Cancer Center 333 Cottman Avenue Philadelphia, PA 19111-2497 Phone: (215) 214-4218 Fax: (215) 728-3616 Email: Edna.Cukierman@fccc.edu.
[1]Equally contributed

BACKGROUND

Ovarian cancer is the most lethal among gynecological malignancies in the United States. About 22,430 new cases and 15,280 deaths from ovarian cancer were estimated for 2007 [1]. More than 70% of patients with epithelial ovarian cancer are diagnosed at an advanced stage when the disease has already spread throughout the peritoneal cavity. Although there has been an improvement in the five-year survival rate for patients diagnosed with advanced, stage III disease, the long-term survival rate is only 15-25% [2]. Although about 75% of patients initially respond to primary therapy, the majority of patients eventually progress and require additional chemotherapy. Unfortunately, second and third-line (and beyond) therapies are aimed at palliative care to prolong time of progression and improve quality of life. Uncontrolled metastases account for the majority of the morbidity and death associated with ovarian cancer. A better understanding of the development and progression of the disease will most likely result in new approaches to treat this aggressive cancer.

One poorly studied aspect of ovarian tumorigenesis is the tumor-stromal interaction. It has become clear that the tumor microenvironment (including stromal fibroblasts, infiltrating immune cells, blood and lymphatic vascular network, and the extracellular matrix (ECM)) is an integral part of the carcinogenic process promoting cell growth and metastases [3-6]. Benign epithelial tumors are constrained by a surrounding stroma [7] that contains fibroblastic cells and a fibrillar three-dimensional (3-D) ECM. These ‘normal’ fibroblasts and ECMs assist in maintaining a homeostatic equilibrium, exerting an inhibitory effect on the epithelial cells undergoing malignant changes [8,9]. However, tumor-generated paracrine signaling alters and overcomes this stromal barrier, inducing changes that promote rather than impede tumor progression [10-13].

Changes in the stroma accompanying tumor progression include emergence of discontinuities in the basement membrane surrounding the growing tumor, severe immune responses, and the formation of new blood vessels (angiogenesis). Among these host responses, additional alterations to the mesenchymal connective tissue appear in the vicinity of the tumor [14-21]. These changes resemble the tissue responses observed during wound healing or fibrosis [22, 23]. In the course of this parallel progression, differentiated myofibroblastic stromal cells (termed tumor-or carcinoma-associated fibroblasts) begin to increase expression of a set of proteins including type I collagen, smooth muscle α-actin (α-SMA) [23], and others [24], thus grossly altering the protein constituents and architecture of both mesenchymal cells and ECM. During this later ‘activated’ stroma phase, the tumor becomes invasive and metastatic [23, 25,26].

Many human tumors are characterized by the progression of their stroma to an activated stage [27-29]. Desmoplasia, the development of an activated (fibrous or desmoplastic) tumor-promoting stroma, occurs in association with invasive cancers of the ovary, breast, prostate, pancreas, gastrointestinal tract, lung, squamous cell carcinomas, and others [3,14,15,23,29, 30]. This stroma often represents more than 50% of the tumor mass, and is associated with a poor prognosis [9,31,32] marked by increased cancer progression to metastasis [24,33-35]. The study of fibroblasts and their role in tumorigenesis has been proposed with the aim of developing treatment strategies to target tumor stroma [36-38], i.e., the tumor-associated fibroblasts or their self-modified microenvironment [36,39]. Successful inhibition of pro-tumorigenic signals from such fibroblasts could replace or complement therapies directed at the malignant cells themselves. In order to develop such therapies, it is essential to use rigorous biochemical methods to characterize tumor-specific fibroblastic stroma to minimize unwanted side effects to host bystander tissue.

At present, we know very little about ovarian fibroblastic stromal activation due to the lack of a suitable, physiologically relevant experimental system. We have previously described the development of a murine *in vivo*-like 3-D stromal system derived from squamous cell carcinoma-associated fibroblasts, which effectively recapitulate their *in vivo* counterparts in a self-derived 3-D matrix dependent manner [40]. Extending this approach in this study, human ovarian fibroblasts were harvested from fresh surgical normal or cancerous ovaries. These harvested human ovarian fibroblasts formed self-derived matrices that effectively resulted in the production of an *in vitro* 3-D matrix system reminiscent of *in vivo* ovarian tumor-associated stroma. We suggest that 3-D matrix-dependent characteristics of harvested fibroblasts can be used to effectively sort these cells as 'normal', 'primed' or 'activated' ovarian fibroblasts. We believe that an *in vivo*-like ovarian stroma 3-D system will enable researchers to study ovarian stromal progression, and to begin to uncover mechanisms that promote ovarian tumor development, progression, and metastasis.

MATERIALS & METHODS

Antibodies

Mouse anti-α-SMA (1:4000, Western blot; 1:300, immunofluorescence; 1:200, immunohistochemistry) and rabbit anti-human fibronectin (1:100, immunofluorescence) were obtained from Sigma-Aldrich (St. Louis, MO), mouse anti-total FAK (1:1000, Western blot) from Millipore (Billerica, MA) and rabbit anti-pFAK^{397} (1:500, Western blot; 1:50, immunohistochemistry) from Invitrogen (Carlsbad, CA). Rabbit anti-Vimentin (1:3000, Western blot) was obtained from Biovision (Mountain View, CA), mouse anti-pan Keratin (1:5000, western blot) from Abcam (Cambridge, MA) and mouse anti-GAPDH (1:10,000, Western blot) from Millipore. Goat anti-mouse IRDye 680 and goat anti-rabbit IRDye 800 from LI-COR biosciences (Lincoln, NE) were used for infrared Western blot detection at 1:10,000. Anti-mouse Rhodamine red and anti-rabbit Cy5, conjugated affinity purified donkey F(ab')2 fragments (1:100, immunofluorescence) were obtained from Jackson Immunoresearch Laboratories (West Grove, PA). Anti-rabbit and anti-mouse, Zymax goat biotinylated IgG (1:1000, immunohistochemistry) were obtained from Invitrogen.

Tissue

Ovarian specimens were obtained with IRB approval from Fox Chase Cancer Center's Biosample Repository. Five tumor and fourteen normal ovarian samples were obtained. The tumor samples were surgically removed from ovarian tumor sites whereas the controls came from non-cancerous prophylactic oophorectomy specimens. Twenty mine (29) tumor and 14 normal ovarian primary fibroblastic cell lines (TOFs and NOFs, respectively) were derived from the above. All the normal and 8 tumor-derived cell lines were selected for further study, according to their morphology. Paraffin-embedded, 5 μm thick, tissue sections corresponding to the fresh tissue specimens were used for immunohistochemical analysis (see **Immunohistochemistry** below).

Isolation of Primary Fibroblasts

Fibroblasts were isolated as described [40,41]. Specifically, under sterile conditions, tissue culture treated 12-well plates were scratched in hashed patterns, rinsed with Phosphate-Buffered Saline (PBS) to remove plastic shavings, and tumor pieces of approximate 1mm^3 size were placed into the wells on the scratched areas, one piece per well. A small amount, 250μl approximately, of medium comprised of high glucose Dulbecco's modified Eagle's medium (Mediatech Inc., Manassas, VA) containing 10% fetal bovine serum (Hyclone, South Logan, UT), 100 U/ml penicillin, and 100 μg/ml streptomycin (DMEM complete), was added to each well and plates were incubated in a humidified 37°C, 10% CO_2 incubator for 2 hours to facilitate tissue adherence. Once the tissue appeared to be attached, more medium (1ml total

volume) was added gently to the tissue pieces and the plates were returned to the incubator. Specimens were inspected daily for the emergence of fibroblasts and media were changed every 3 days. Fibroblasts were transferred to larger tissue culture vessels once they had reached confluency, after approximately 2 weeks. All fibroblasts used for this study were between passages 3 and 5.

Production of fibroblast-derived unextracted 3-D matrices

Isolated primary fibroblasts were induced to secrete and organize their own 3-D *in vivo*-like matrices as previously described [40-42]. Briefly, 250,000 cells/ml were plated on chemically cross-linked gelatin-coated tissue culture dishes, or coverslips, and maintained in a state of confluency for 6-8 days, supplemented every 48 hours with 50 μg/ml fresh L-ascorbic acid (Sigma-Aldrich). At the end of this period, the resultant "unextracted 3-D matrix" cultures were either lysed for Western blot or stained for immunofluorescence analyses (see **Indirect immunofluorescence**). For 2-D cultures, isolated fibroblasts were plated at 100,000 cells/ml density and cultured overnight in DMEM complete (see **Isolation of Primary Fibroblasts**) on tissue culture treated plastic astic dishes before they were further characterized.

Indirect immunofluorescence

Unextracted fibroblast-derived 3-D matrices cultured on glass coverslips were fixed, permeabilized and stained according to standard procedures [40,41,43]. Briefly, blocking was performed using M.O.M ("Mouse on Mouse") mouse IgG blocking reagent (M.O.M. kit BMK-2202, Vector Laboratories, Burlingame, CA) supplemented with 20% normal donkey serum (Jackson Immunoresearch Laboratories) in PBS, inside a humidified chamber for 1 hour at 37°C. After washing, an incubation at room temperature for 5 minutes with 8% M.O.M. protein concentrate (M.O.M. kit BMK-2202, Vector Laboratories) and 5% normal donkey serum in PBS (antibody incubation media), was followed by staining with rabbit anti-human fibronectin (1:100) and mouse anti-α-SMA (1:300) in antibody incubation media. After washing, coverslips were incubated with anti-rabbit Cy5 and anti-mouse Rhodamine Red conjugated donkey F(ab')2 fragments (1:100) and SYBR Green nuclear stain (1:50,000, Invitrogen) in 10% normal donkey serum PBS-Tween 20 (Sigma-Aldrich) for 30 minutes at room temperature. Coverslips were then washed and mounted using Prolong gold (Invitrogen) anti-fading reagent.

Image Acquisition and Reconstitution

Three-dimensional immunofluorescently stained pre-extracted matrix samples (unextracted 3-D matrices) were imaged using an Ultraview spinning-disc confocal (Perkin-Elmer Life Sciences, Boston, MA) paired to a Nikon TE-2000U microscope (Optical Apparatus Co., Ardmore, PA). Sequential images, at three different wavelengths, were captured at 0.5 μm-thick Z-slices using the company's software. Maximum reconstruction of planes was performed using MetaMorph offline 7.0r1 imaging analysis softwareftware (Molecular Devices, Downingtown, PA).

Two-dimensional cultures were imaged using a Nikon TE-2000U wide field inverted microscope (Optical Apparatus Co., Ardmore, PA) with a Roper Scientific Cool Snap HQ camera. Captures were taken using MetaMorph offline 6.2r1 imaging analysis software.

Quantitative Western blotting

Cells from both 2-D and 3-D cultures were lysed and the lysates were resolved by SDS-PAGE (sodium dodecyl sulfate-polyacrylamide electrophoresis) and transferred, as previously described [40,41]. Blocking was performed overnight, at 4°C, using Odyssey Blocking Buffer. Blots were then incubated with a combination of primary antibodies against α-SMA (1:4000),

total FAK (1:1000), pFAKY^{397} (1:500), Vimentin (1:3000), pan-Keratin (1:5000) and GAPDH (1:10,000) in Odyssey Blocking Buffer with 0.05% Tween-20, for 2 hours at room temperature. After three 15-minute washes in Tris-Buffered Saline Tween-20 (TBST), the blots were incubated with secondary antibodies, IRDye 680 goat anti-mouse and IRDye 800 goat anti-rabbit (1:10,000, LI-COR) in Odyssey Blocking Buffer supplemented with 0.05% Tween-20 and 0.01% SDS (Sigma-Aldrich), for 2 hours at room temperature. After three 10-minute washes in TBST, blots were transferred in TBS and scanned using the Odyssey Infrared Imaging System (LI-COR) following the Odyssey User Guide's (version 2.1) instructions for membranes. A minimum of two independent analyses were performed for each fibroblastic cell line. Results were quantified using the Odyssey 2.1.12 application software, with median background subtraction and 3 points selected border width. Ratios were calculated and histograms created using MS-Excel 2002 (Microsoft Corp., Redmond, WA).

Immunohistochemistry

Paraffin-embedded sections were deparaffinized in xylene and rehydrated in a graded series of ethanol and water. For antigen retrieval, sections were boiled in 10 mM sodium citrate-buffer (Thermo Fisher Scientific, Waltham, MA) pH 6.0, for 8 min. Endogenous peroxidase activity was blocked with 3% hydrogen peroxide (Sigma-Aldrich) in PBS for 30 min at room temperature. Nonspecific background was eliminated incubating the tissue with 5% normal goat serum (Sigma-Aldrich) in PBS for 30 min at room temperature, followed by streptavidin and biotin blocking according to the manufacturer's instructions (Vector Laboratories). Sections were then incubated in a humidified chamber with rabbit anti-pFAKY^{397} (1:50) or mouse anti-α-sma (1:200) antibodies overnight at 4°C. Zymax goat anti-rabbit and anti-mouse biotinylated IgG secondary antibodies (Invitrogen) were used at 1:1000 dilution. The samples were then labeled with HRP-conjugated streptavidin (Invitrogen) and the chromogenic reaction developed using Liquid DAB Substrate Pack (Biogenex, San Ramon, CA) according to the manufacturer's instructions. Sections were counterstained using Harris modified hematoxylin (Thermo Fisher Scientific). Negative controls included omission of the primary antibodies and substitution of the primary antibodies with normal rabbit and mouse IgG (Sigma-Aldrich).

RESULTS

Primary ovarian fibroblasts cultured under 2-D conditions, present three distinct morphological phenotypes

Table 1 lists 14 normal ovarian fibroblast (NOF) cell lines derived from 14 postmenopausal non-cancerous ovaries (from patients aged 55.7 +/− 8 years) that were incidentally resected during laparotomies from patients with high risks of developing ovarian cancers (i.e., based on BRCA1/2 mutational status). In addition, Table 1 also lists 29 tumor ovarian fibroblast (TOF) cell lines from 5 distinct surgical ovarian tumor samples (from patients aged 57.4 +/− 17 years), which were harvested as previously described (see Materials and Methods in [40, 41]). When cultured under traditional 2-D conditions, these fibroblasts presented three distinguishable morphologies. The first morphology was elongated, and almost needle-like. This was seen in three cell lines from the same patient, and was designated as ‘spindle.’ The second, seen in one cell line, was more elliptical in shape, and was classified as ‘intermediate.’ The third was broad and flat, and was designated ‘spread’. In sum, the TOFs had (3) spindle, (25) spread, and (1) intermediate cell-line morphologies (Figure 1 and Table 1). In contrast, all NOFs were ‘spread’, and were morphologically indistinguishable from each other.

Two spindle (1a and 1b), the single intermediate (2a) and 4 spread (2b, 2c, 3a and 3b) TOFs, together with the 14 NOFs (6-20), were selected for further characterization. In order to confirm that the harvested cells were indeed fibroblasts, cells were cultured on conventional 2-D conditions overnight, and cell lysates subsequently analyzed by Western blot, using antibodies

recognizing vimentin as fibroblastic and keratin as epithelial cell markers. The human primary fibroblastic cell line, WI38 was used as positive control, while the epithelial human tumorigenic MCF7 line was used as negative control. One cell line, (2c), was positive for both vimentin and keratin expression, and therefore was not characterized further. Figure 2 shows representative fibroblastic and non fibroblastic cell line identifications.

ECM-dependent biochemical differences between NOFs and TOFs mark the distinct morphological classes

Fibroblasts were maintained for 8 days at confluent cell concentrations under matrix-stabilizing conditions [41,42]. At the end of the 8-day period, unextracted 3-D cultures, where cells grow on a substrate made of their own secreted ECM, were obtained [40,43]. As controls, all fibroblasts were also cultured under conventional 2-D conditions (see Materials and Methods). Western blot analysis of cell lysates from 2-D- and unextracted 3-D-cultured cells was performed with antibodies to α-SMA, focal adhesion kinase (FAK), and $pFAKY^{397}$.

α-SMA is a marker of myofibroblastic differentiation, and is expressed *in vivo* by activated (e.g., desmoplastic) tumor- or carcinoma-associated fibroblasts [23,44,45]. We have recently shown (using a murine squamous cell carcinoma system) that levels of α-SMA expression are 3-D matrix dependent [40]. Proto-myofibroblastic cells are known to be 'primed' or pre-myofibroblastic cells that down-regulate α-SMA expression before differentiation into myofibroblastic cells [45]. Further, expression of α-SMA in normal ovarian fibroblast has been previously reported in some parts of the normal ovary [46]. Separately, we and others have shown that while total levels of FAK expression remain unchanged in fibroblastic 2-D vs. 3-D cultures, the levels of tyrosine phosphorylated (activated) $pFAKY^{397}$ is greater in 2-D culture conditions [43,47-55]. The housekeeping protein glyceraldehyde 3-phosphate dehydrogenase (GAPDH) was used as a loading control.

We calculated the averages of α-SMA 287 expression levels (normalized to GAPDH) and the pFAK/tFAK ratios for the NOFs and TOFs. Figure 3A shows that there were no significant differences between 2-D and unextracted 3-D cultures, or between the NOF and TOF populations, in expression of both α-SMA and pFAK/tFAK ratios. Next, we sorted the NOFs in to BRCA1/2 mutant vs. wild type groups (see Table 1). Again, no differences between these populations were observed (Figure 3B). We then sorted all fibroblasts (NOFs and TOFs) based on their morphology (Table 1) and again compared them as above. Figure 3C shows that 'spread' (including both NOF and TOF samples) and 'spindle' (TOFs) populations are similar to each other in expressing high levels of α- SMA, which correlated with high pFAK/tFAK ratios, paralleling studies of myofibroblastic differentiation in other systems [56-58]. Interestingly, the single TOF line that was morphologically intermediate showed 3-D matrix-dependent low α-SMA expression and pFAK/tFAK ratios corresponding to our previously reported primed 3-D cultures [40, 41, 43, 47]. These results are summarized in Table 2 while representative Western blots are shown in Figure 4.

Confocal microscopy analyses of unextracted 3-D cultures are necessary to characterize primary ovarian fibroblasts as 'normal,' 'primed' or 'activated '

To test whether the observed morphological features of cells, cultured under conventional 2-D conditions, are sufficient (or not) to predict whether the assorted TOFs are normal, primed, or activated (e.g., desmoplastic and myofibroblastic), we conducted indirect immunofluorescence analyses. In this assay, we simultaneously scanned triple labeled images using a spinning disc confocal microscope equipped with lasers to excite and emit three individual wavelengths (see Materials and Methods). We have reported that unextracted normal and primed cultures present disorganized ECMs, and dense cultures of cells with relatively round nuclei, while activated (e.g., desmoplastic or myofibroblastic) unextracted

cultures produce signature parallel 3-D matrix patterns while their nuclei are condensed, elliptical and organized in the same orientation as their ECMs [40,41]. In addition, it has been reported that while α-SMA expression is heterogeneously expressed in normal ovarian tissues [46], primed unextracted cultures down regulate α-SMA expression levels [40,41], similarly to proto-myofibroblastic cells [45,59]. In contrast, activated myofibroblasts (e.g., desmoplastic), homogenously express α-SMA in an intense stress fiber-like pattern [59,60]. Therefore, in our analysis we simultaneously labeled ECM (fibronectin), nuclei (DNA), and α-SMA. Figure 5 shows three individual populations, which were positively sorted due to their matrix, nuclei and α-SMA characteristics as 'normal,' 'primed' or 'activated' (e.g., myofibroblastic or desmoplastic).

Next, we asked if the morphological and biochemical features correlated with the indirect immunofluorescence patterns. We observed that while NOFs were sorted as 'normal,' the TOFs that originally presented spread and spindle morphologies were indistinguishable from each other yet very different from all NOFs, in unextracted 3-D cultures and, thus, sorted as 'activated.' Figure 6 depicts the biochemical analyses using 'normal,' 'primed' or 'activated' sorting.

Matrix-dependent characteristics of ovarian 'normal,' 'primed' and 'activated' fibroblastic 3-D cultures are reminiscent of their *in vivo* counterparts

To extend our observations and assess the physiological and pathological relevance of unextracted cultures, we tested paraffin-embedded samples of some of the normal and cancerous tissues from which the fibroblast cell lines were harvested. Samples corresponding to numbers 1, 2 and 8 (see Table 1), were immunohistochemically labeled to identify the localization and intensities of $pFAKY^{397}$ and α-SMA, and counterstained using hematoxylin (see Materials and Methods).

Figure 7 shows that *in vivo* mesenchymal ovarian tissue with high α-SMA expression (e.g., normal and activated or myofibroblastic stroma) correlated with high levels of $pFAKY^{397}$, while low α-SMA levels (indicating primed or proto-myofibroblastic stroma) correlated with low $pFAKY^{397}$ levels. Table 3 summarizes these observations, which suggest that conventional 2-D culture morphological features, as well as biochemical analyses are sufficient to identify the intermediate stage 'primed' fibroblasts; while indirect immunofluorescence analyses of the unextracted 3-D cultures confirmed the 'primed' phenotype and effectively sorted 'normal' away from 'activated' 3-D cultures.. These observations confirmed that 'normal,' 'primed' and 'activated' fibroblasts *in vitro* maintain their *in vivo* characteristics in a 3-D matrix dependent manner. Therefore, we believe that results from the immunohistochemical analyses validate this staged stromal 3-D approach as a physiologically relevant *in vivo*-like system.

DISCUSSION

It is increasingly recognized that interactions between cancer cells and their surrounding stroma are critical for promoting the growth and invasiveness of tumors [10,11,61-63]. For example, cancer cells alter the topography and molecular composition of stromal ECM by paracrine regulation of fibroblastic stromal cells [64] during early tumor development. These physical and biochemical alterations of the stroma, in turn, profoundly affect the properties of the cancer cells [10,55,65]. The vital interplay between tumor and stroma means that, in principle, it is possible to target signaling pathways that regulate tumor-induced stroma progression and, in this way, contain tumorigenesis [36,39,66-70]. To achieve this, an *in vivo*-like, progressive stromal model system in ovarian malignancies is needed to facilitate the study of mechanisms that support and induce metastatic behavior and are responsible for stroma permissiveness. This study, for the first time, reports the development of such an *in vivo*-like 3-D stromal model system.

Our data suggest that although fibroblasts harvested from postmenopausal normal and neoplastic ovarian samples present three clear morphologies, biochemical analyses comparing 2-D and 3-D cultures, as well as confocal studies of unextracted 3-D cultures are needed in order to sort these as 'normal,' 'primed' or 'activated' fibroblasts. For example, fibroblasts presenting spread morphology were sorted as 'normal' or 'activated,' while all spindle cells were sorted as 'activated' and the single intermediate morphology cell-line was characterized as 'primed.' Note that this study does not rule out the possibility that the single intermediate-morphology cell characterized as 'primed,' is in fact representative of an additional stromal phenotype (e.g., oncofetal [71-73] as opposed to desmoplastic). The reason for characterizing the single intermediate cell type as 'primed' (as opposed to oncofetal 'activated'), is that the same tumor sample, #2, rendered additional cells presenting a spread morphology (Table 1), which were sorted as desmoplastic 'activated' and, to our knowledge, the literature, has not identified desmoplastic and oncofetal stromas to coincide at a single tumor location [3,14]. Moreover, attempts to confirm oncofetal marker expression such as oncofetal fibronectin were not successful (not shown). Nevertheless, there is no question that this cell type indeed represents a discrete stromal setting that differs from both normal and desmoplastic ('active' or myofibroblastic) microenvironments and, as such, it might represent the early predisposed stromal stage identified *in vivo* as 'primed stroma'.

Moreover, it is important to underline that the goal of this study is not to provide statistics regarding the confidence of sorting cells by their morphology, biochemistry and unextracted 3-D topography; instead, the study aims at stressing the importance of establishing a reliable 3-D system model that effectively mimics progressive stages of human ovarian cancer-associated stroma *in vivo*. Historically, harvesting and culturing of fibroblasts (and additional cells) has taken place in conventional tissue culture plates (or flasks). Therefore, fibroblasts plated onto plastic dishes represent a 2-D system resulting in an artificially polarized culture with distinctive dorsal and ventral divergence [47,49,54,74-77]. We, and others, have shown that cells grown on 2-D cultures have both biochemical and morphological altered phenotypes that greatly differ from their *in vivo* counterparts [6,47,49,55,78-81]. Given that cell-matrix interactions are different in 2-D and 3-D systems, we have developed a model system where fresh ovarian tissue samples are used to harvest normal- and/or tumor-associated fibroblasts. These fibroblasts, in turn, derive an *in vitro*, but still physiologically relevant, 3-D scaffold (matrix) that effectively mimics a number of *in vivo* ovarian stromal microenvironmental settings, as shown herein by the immunohistochemistry analyses.

Fibroblasts, within the stroma, have been shown to undergo both structural and biochemical alterations based on their relationship to cancer cells [14,15,23]. Among the goals of this study was to determine if f fibroblasts could be harvested from postmenopausal yet normal or pathologically identified as non-cancerous ovaries (from individuals considered to be at a high risk for ovarian cancer) and ovarian tumor specimens, to characterize these fibroblasts and question whether they can reconstitute a progressive staged 3-D model system that recapitulates its *in vivo* counterparts. Once the *in vivo*-like relevance is established, this model system can begin to be used for characterization of the progressive stromal changes that occur in the ovarian tissue during tumor development. Characterizing stroma, particularly stroma directly adjacent to tumor and presumably permissive or primed to promote tumor growth, may facilitate the use of chemotherapeutic agents directed against it. Use of the 3-D matrix model system would allow for a more *in vivo*-like representation of both stromal fibroblast and stroma-induced cancer cell behaviors. In theory, such a technique is attractive in the sense that therapy can be (in the future) tailored and, thus, directed towards patient-specific cell phenotypes. Although much study is needed in order to use this model system for diagnosis or prognosis, we believe that it constitutes the basis for the future development of such tools.

ACKNOWLEDGMENTS

We thank Dr. A. Klein-Szanto for assistance in pathological observations of immunohistochemistry assays, Ms. C. M. Slater for her expertise in tissue culture, Mrs. O. Villamar for assistance on immunohistochemistry techniques, Drs. R. Castelló-Cros and G. P. Adams, for critical comments, Ms. R. Roth for technical assistance and Mrs. K. Buchheit for proofreading. This study was assisted by the following Fox Chase Cancer Center facilities: Biosample Repository, Histopathology Facility, Cell Culture, Glass-Washing and the Talbot Research Library. In addition, funds supporting this work were obtained from the American Association of Cancer Research (the department specifically disclaims responsibility for any analyses, interpretations, or conclusions), the WW Smith Charitable Trust, the Ovarian Cancer Research Fund, the Ovarian Cancer SPORE at FCCC (P50 CA083638), grants RO1-CA113451 and CA-06927 from the NCI, as well as an appropriation from the Commonwealth of Pennsylvania.

REFERENCES

1. Jemal A, Siegel R, Ward E, Murray T, Xu J, Thun MJ. Cancer statistics, 2007. CA Cancer J Clin 2007;57(1):43–66. [PubMed: 17237035]
2. Ozols RF, Bookman MA, Connolly DC, Daly MB, Godwin AK, Schilder RJ, et al. Focus on epithelial ovarian cancer. Cancer Cell 2004;5(1):19–24. [PubMed: 14749123]
3. Beacham DA, Cukierman E. Stromagenesis: The changing face of fibroblastic microenvironments during tumor progression. Semin Cancer Biol 2005;15(5):329–41. [PubMed: 15970443]
4. Albini A, Sporn MB. The tumour microenvironment as a target for chemoprevention. Nat Rev Cancer 2007;7(2):139–47. [PubMed: 17218951]
5. Li H, Fan X, Houghton J. Tumor microenvironment: The role of the tumor stroma in cancer. J Cell Biochem 2007;101(4):805–15. [PubMed: 17226777]
6. Bissell MJ. Modelling molecular mechanisms of breast cancer and invasion: Lessons from the normal gland. Biochem Soc Trans 2007;35(Pt 1):18–22. [PubMed: 17212581]
7. Parrott JA, Nilsson E, Mosher R, Magrane G, Albertson D, Pinkel D, et al. Stromal-epithelial interactions in the progression of ovarian cancer: Influence and source of tumor stromal cells. Mol Cell Endocrinol 2001;175(12):29–39. [PubMed: 11325514]
8. Kuperwasser C, Chavarria T, Wu M, Magrane G, Gray JW, Carey L, et al. Reconstruction of functionally normal and malignant human breast tissues in mice. Proc Natl Acad Sci 2004;101(14): 4966–71. [PubMed: 15051869]
9. Bissell MJ, Radisky D. Putting tumours in context. Nat Rev Cancer 2001;1(1):46–54. [PubMed: 11900251]
10. Bhowmick NA, Moses HL. Tumor-stroma interactions. Curr Opin Genet Dev 2005;15(1):97–101. [PubMed: 15661539]
11. Glick AB, Yuspa SH. Tissue homeostasis and the control of the neoplastic phenotype in epithelial cancers. Semin Cancer Biol 2005;15(2):75–83. [PubMed: 15652452]
12. Maffini MV, Soto AM, Calabro JM, Ucci AA, Sonnenschein C. The stroma as a crucial target in rat mammary gland carcinogenesis. J Cell Sci 2004;117(8):1495–502. [PubMed: 14996910]
13. Kalluri R, Zeisberg M. Fibroblasts in cancer. Nat Rev Cancer 2006;6(5):392–401. [PubMed: 16572188]
14. Kunz-Schughart LA, Knuechel R. Tumor-associated fibroblasts (part i): Active stromal participants in tumor development and progression? Histol Histopathol 2002;17(2):599–621. [PubMed: 11962761]
15. Kunz-Schughart LA, Knuechel R. Tumor-associated fibroblasts (part ii): Functional impact on tumor tissue. Histol Histopathol 2002;17(2):623–37. [PubMed: 11962762]
16. Thomas GJ, Hart IR, Speight PM, Marshall JF. Binding of tgf-beta1 latency associated peptide (lap) to alpha(v)beta6 integrin modulates behaviour of squamous carcinoma cells. Br J Cancer 2002;87 (8):859–67. [PubMed: 12373600]
17. Hauptmann S, Siegert A, Berger S, Denkert C, Kobel M, Ott S, et al. Regulation of cell growth and the expression of extracellular matrix proteins in colorectal adenocarcinoma: A fibroblast-tumor cell coculture model to study tumor-host interactions in vitro. Eur J Cell Biol 2003;82(1):1–8. [PubMed: 12602943]

18. Kaarteenaho-Wiik R, Soini Y, Pollanen R, Paakko P, Kinnula VL. Over expression of tenascin-c in malignant pleural mesothelioma. Histopathology 2003;42(3):280–91. [PubMed: 12605648]
19. Slater MD, Lauer C, Gidley-Baird A, Barden JA. Markers for the development of early prostate cancer. J Pathol 2003;199(3):368–77. [PubMed: 12579539]
20. De Santis R, Anastasi AM, D'Alessio V, Pelliccia A, Albertoni C, Rosi A, et al. Novel antitenascin antibody with increased tumour localisation for pretargeted antibody guided radioimmunotherapy (pagrit(r)). Br J Cancer 2003;88(7):996–1003. [PubMed: 12671694]
21. Kalembeyi I, Inada H, Nishiura R, Imanaka-Yoshida K, Sakakura T, Yoshida T. Tenascin-c upregulates matrix metalloproteinase-9 in breast cancer cells: Direct and synergistic effects with transforming growth factor beta1. Int J Cancer 2003;105(1):53–60. [PubMed: 12672030]
22. Dvorak HF. Tumors: Wounds that do not heal. Similarities between tumor stroma generation and wound healing. N Engl J Med 1986;315(26):1650–59. [PubMed: 3537791]
23. Desmouliere A, Guyot C, Gabbiani G. The stroma reaction myofibroblast: A key player in the control of tumor cell behavior. Int J Dev Biol 2004;48(56):509–17. [PubMed: 15349825]
24. Binkley CE, Zhang L, Greenson JK, Giordano TJ, Kuick R, Misek D, et al. The molecular basis of pancreatic fibrosis: Common stromal gene expression in chronic pancreatitis and pancreatic adenocarcinoma. Pancreas 2004;29(4):254–63. [PubMed: 15502640]
25. Chung LW, Baseman A, Assikis V, Zhau HE. Molecular insights into prostate cancer progression: The missing link of tumor microenvironment. J Urol 2005;173(1):10–20. [PubMed: 15592017]
26. Hsu MY, Meier F, Herlyn M. Melanoma development and progression: A conspiracy between tumor and host. Differentiation 2002;70(910):522–36. [PubMed: 12492494]
27. Cunha GR, Matrisian LM. It's not my fault, blame it on my microenvironment. Differentiation 2002;70 (910):469–72. [PubMed: 12492489]
28. Olumi AF, Grossfeld GD, Hayward SW, Carroll PR, Tlsty TD, Cunha GR. Carcinoma-associated fibroblasts direct tumor progression of initiated human prostatic epithelium. Cancer Res 1999;59 (19):5002–11. [PubMed: 10519415]
29. Omary MB, Lugea A, Lowe AW, Pandol SJ. The pancreatic stellate cell: A star on the rise in pancreatic diseases. J Clin Invest 2007;117(1):50–59. [PubMed: 17200706]
30. Tuxhorn JA, Ayala GE, Smith MJ, Smith VC, Dang TD, Rowley DR. Reactive stroma in human prostate cancer: Induction of myofibroblast phenotype and extracellular matrix remodeling. Clin Cancer Res 2002;8(9):2912–23. [PubMed: 12231536]
31. Cheng JD, Weiner LM. Tumors and their microenvironments: Tilling the soil. Commentary re: A. M. Scott et al., a phase i dose-escalation study of sibrotuzumab in patients with advanced or metastatic fibroblast activation protein-positive cancer. Clin. Cancer res., 9: 1639-1647, 2003. Clin Cancer Res 2003;9(5):1590–95. [PubMed: 12738710]
32. Barsky SH, Green WR, Grotendorst GR, Liotta LA. Desmoplastic breast carcinoma as a source of human myofibroblasts. Am J Pathol 1984;115(3):329–33. [PubMed: 6329001]
33. Tuxhorn JA, Ayala GE, Rowley DR. Reactive stroma in prostate cancer progression. J Urol 2001;166 (6):2472–83. [PubMed: 11696814]
34. Edlund M, Sung SY, Chung LW. Modulation of prostate cancer growth in bone microenvironments. J Cell Biochem 2004;91(4):686–705. [PubMed: 14991761]
35. Hasebe T, Sasaki S, Imoto S, Ochiai A. Highly proliferative fibroblasts forming fibrotic focus govern metastasis of invasive ductal carcinoma of the breast. Mod Pathol 2001;14(4):325–37. [PubMed: 11301349]
36. Liotta LA, Kohn EC. The microenvironment of the tumour-host interface. Nature 2001;411(6835): 375–79. [PubMed: 11357145]
37. Sung SY, Chung LW. Prostate tumor-stroma interaction: Molecular mechanisms and opportunities for therapeutic targeting. Differentiation 2002;70(910):506–21. [PubMed: 12492493]
38. Mersmann M, Schmidt A, Rippmann JF, Wuest T, Brocks B, Rettig WJ, et al. Human antibody derivatives against the fibroblast activation protein for tumor stroma targeting of carcinomas. Int J Cancer 2001;92(2):240–8. [PubMed: 11291052]
39. Simberg D, Duza T, Park JH, Essler M, Pilch J, Zhang L, et al. Biomimetic amplification of nanoparticle homing to tumors. Proc Natl Acad Sci USA 2007;104(3):932–36. [PubMed: 17215365]

40. Amatangelo MD, Bassi DE, Klein-Szanto AJ, Cukierman E. Stroma-derived three-dimensional matrices are necessary and sufficient to promote desmoplastic differentiation of normal fibroblasts. Am J Pathol 2005;167(2):475–88. [PubMed: 16049333]
41. Castelló-Cros, R.; Cukierman, E. Stromagenesis during tumorigenesis: Characterization of tumor-associated fibroblasts and stroma-derived 3d matrices. In: Even-Ram, S., editor. Methods mol biol / extracellular matrix protocols. Totowa, NJ: Humana Press; 2008. in press
42. Beacham, DA.; Amatangelo, MD.; Cukierman, E. Preparation of extracellular matrices produced by cultured and primary fibroblasts. In: Bonifacino, JS.; Dasso, M.; Lippincott-Schwartz, J.; Harford, JB.; Yamada, KM., editors. Curr protocols cell biol. John K. Wiley & Sons: 2006. p. 10.09.01-10.09.21.
43. Cukierman E, Pankov R, Stevens DR, Yamada KM. Taking cell-matrix adhesions to the third dimension. Science 2001;294(5547):1708–12. [PubMed: 11721053]
44. Yazhou C, Wenlv S, Weidong Z, Licun W. Clinicopathological significance of stromal myofibroblasts in invasive ductal carcinoma of the breast. Tumour Biol 2004;25(56):290–95. [PubMed: 15627894]
45. Gabbiani G. The myofibroblast in wound healing and fibrocontractive diseases. J Pathol 2003;200 (4):500–03. [PubMed: 12845617]
46. Santini D, Ceccarelli C, Leone O, Pasquinelli G, Piana S, Marabini A, et al. Smooth muscle differentiation in normal human ovaries, ovarian stromal hyperplasia and ovarian granulosa-stromal cells tumors. Mod Pathol 1995;8(1):25–30. [PubMed: 7731938]
47. Cukierman E, Pankov R, Yamada KM. Cell interactions with three-dimensional matrices. Curr Opin Cell Biol 2002;14(5):633–40. [PubMed: 12231360]
48. Yamada KM, Pankov R, Cukierman E. Dimensions and dynamics in integrin function. Braz J Med Biol Res 2003;36(8):959–66. [PubMed: 12886449]
49. Yamada K, M. Cukierman E. Modeling tissue morphogenesis and cancer in 3d. Cell 2007;130(4): 601–10. [PubMed: 17719539]
50. Li S, Lao J, Chen BPC, Li Y-S, Zhao Y, Chu J, et al. Genomic analysis of smooth muscle cells in 3-dimensional collagen matrix. FASEB J 2003;17(1):97–99. [PubMed: 12475912]
51. Wozniak MA, Desai R, Solski PA, Der CJ, Keely PJ. Rock-generated contractility regulates breast epithelial cell differentiation in response to the physical properties of a three-dimensional collagen matrix. J Cell Biol 2003;163(3):583–95. [PubMed: 14610060]
52. Mitra SK, Hanson DA, Schlaepfer DD. Focal adhesion kinase: In command and control of cell motility. Nature Reviews Molecular Cell Biology Nat Rev Mol Cell Biol 2005;6(1):56–68.
53. Winters BS, Raj BKM, Robinson EE, Foty RA, Corbett SA. Three-dimensional culture regulates raf-1 expression to modulate fibronectin matrix assembly. Mol Biol Cell 2006;17(8):3386–96. [PubMed: 16707572]
54. Rhee S, Jiang H, Ho CH, Grinnell F. Microtubule function in fibroblast spreading is modulated according to the tension state of cell-matrix interactions. Proc Natl Acad Sci U S A 2007;104(13): 5425–3540. [PubMed: 17369366]
55. Paszek MJ, Zahir N, Johnson KR, Lakins JN, Rozenberg GI, Gefen A, et al. Tensional homeostasis and the malignant phenotype. Cancer Cell 2005;8(3):241–54. [PubMed: 16169468]
56. Greenberg RS, Bernstein AM, Benezra M, Gelman IH, Taliana L, Masur SK. Fakdependent regulation of myofibroblast differentiation. FASEB J 2006;20(7):1006–08. [PubMed: 16585062]
57. Asano Y, Ihn H, Yamane K, Jinnin M, Tamaki K. Increased expression of integrin alphavbeta5 induces the myofibroblastic differentiation of dermal fibroblasts. Am J Pathol 2006;168(2):499–510. [PubMed: 16436664]
58. Mimura Y, Ihn H, Jinnin M, Asano Y, Yamane K, Tamaki K. Constitutive phosphorylation of focal adhesion kinase is involved in the myofibroblast differentiation of scleroderma fibroblasts. J Invest Dermatol 2005;124(5):886–92. [PubMed: 15854026]
59. Hinz B, Gabbiani G. Mechanisms of force generation and transmission by myofibroblasts. Curr Opin Biotechnol 2003;14:538–46. [PubMed: 14580586]
60. Hinz B. Formation and function of the myofibroblast during tissue repair. J Invest Dermatol 2007;127 (3):526–37. [PubMed: 17299435]
61. Campisi J. Senescent cells, tumor suppression, and organismal aging: Good citizens, bad neighbors. Cell 2005;120(4):513–22. [PubMed: 15734683]

62. Mueller MM, Fusenig NE. Friends or foes - bipolar effects of the tumour stroma in cancer. Nat Rev Cancer 2004;4(11):839–49. [PubMed: 15516957]
63. Li G, Satyamoorthy K, Meier F, Berking C, Bogenrieder T, Herlyn M. Function and regulation of melanoma-stromal fibroblast interactions: When seeds meet soil. Oncogene 2003;22(20):3162–31671. [PubMed: 12789292]
64. Bhowmick NA, Neilson EG, Moses HL. Stromal fibroblasts in cancer initiation and progression. Nature 2004;432(7015):332–37. [PubMed: 15549095]
65. Bhowmick NA, Chytil A, Plieth D, Gorska AE, Dumont N, Shappell S, et al. Tgfbeta signaling in fibroblasts modulates the oncogenic potential of adjacent epithelia. Science 2004;303(5659):848–51. [PubMed: 14764882]
66. Kenny PA, Bissell MJ. Tumor reversion: Correction of malignant behavior by microenvironmental cues. Int J Cancer 2003;107(5):688–95. [PubMed: 14566816]
67. Soto AM, Sonnenschein C. Emergentism as a default: Cancer as a problem of tissue organization. J Biosci 2005;30(1):103–18. [PubMed: 15824446]
68. Baker SG, Kramer BS. Paradoxes in carcinogenesis: New opportunities for research directions. BMC Cancer 2007;7:151. [PubMed: 17683619]
69. Kaspar M, Zardi L, Neri D. Fibronectin as target for tumor therapy. Int J Cancer 2006;118(6):1331–39. [PubMed: 16381025]
70. Fidler IJ. The pathogenesis of cancermetastasis: The ‘seed and soil’ hypothesis revisited. Nature Reviews Cancer 2003;3(6):453–58.
71. Loridon-Rosa B, Vielh P, Matsuura H, Clausen H, Cuadrado C, Burtin P. Distribution of oncofetal fibronectin in human mammary tumors: Immunofluorescence study on histological sections. Cancer Res 1990;50(5):1608–12. [PubMed: 2406016]
72. Matsuura H, Hakomori S. The oncofetal domain of fibronectin defined by monoclonal antibody fdc-6: Its presence in fibronectins from fetal and tumor tissues and its absence in those from normal adult tissues and plasma. Proc Natl Acad Sci U S A 1985;82(19):6517–21. [PubMed: 2995969]
73. Menzin AW, Loret de Mola JR, Bilker WB, Wheeler JE, Rubin SC, Feinberg RF. Identification of oncofetal fibronectin in patients with advanced epithelial ovarian cancer: Detection in ascitic fluid and localization to primary sites and metastatic implants. cancer 1998;82(1):152–58. [PubMed: 9428492]
74. Ahmed I, Ponery AS, Nur EKA, Kamal J, Meshel AS, Sheetz MP, et al. Morphology, cytoskeletal organization, and myosin dynamics of mouse embryonic fibroblasts cultured on nanofibrillar surfaces. Mol Cell Biochem 2007;301(12):241–49. [PubMed: 17294137]
75. Grinnell F, B. Rocha L, Iucu C, Rhee S, Jiang H. Nested collagen matrices: A new model to study migration of human fibroblast populations in three dimensions. Experimental Cell Research 2006;312(1):86–94. [PubMed: 16256985]
76. Tamariz E, Grinnell F. Modulation of fibroblast morphology and adhesion during collagen matrix remodeling. Mol Biol Cell 2002;13(11):3915–29. [PubMed: 12429835]
77. Jiang H, Grinnell F. Cell-matrix entanglement and mechanical anchorage of fibroblasts in three-dimensional collagen matrices. Mol Biol Cell 2005;16(11):5070–76. [PubMed: 16107563]
78. Gospodarowicz D, Greenburg G, Birdwell CR. Determination of cellular shape by the extracellular matrix and its correlation with the control of cellular growth. Cancer Res 1978;38(11 Pt 2):4155–71. [PubMed: 359133]
79. Fischbach C, Chen R, Matsumoto T, Schmelzle T, Brugge JS, Polverini PJ, et al. Engineering tumors with 3d scaffolds. Nat Methods 2007;4(10):855–60. [PubMed: 17767164]
80. Larsen M, Artym VV, Green JA, Yamada KM. The matrix reorganized: Extracellular matrix remodeling and integrin signaling. Current Opinion in Cell Biology 2006;18(5):463–71. [PubMed: 16919434]
81. Pedersen JA, Swartz MA. Mechanobiology in the third dimension. Ann Biomed Eng 2005;33(11): 1469–90. [PubMed: 16341917]

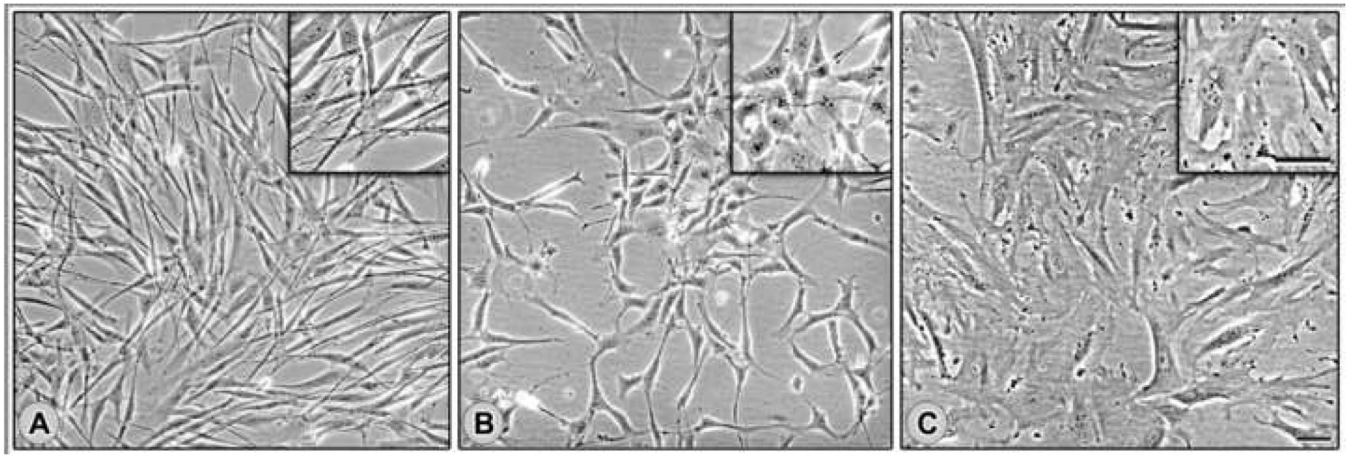

Figure 1. Fibroblasts harvested from human ovarian tissue present, spindle, intermediate or spread morphologies under 2-D conditions

Primary fibroblasts, harvested from fresh ovarian tissue samples (see Materials and Methods), were cultured under traditional 2-D conditions to assess their morphological features. Representative cultures displaying spindle (**A**), intermediate (**B**) and spread (**C**) morphologies are shown.

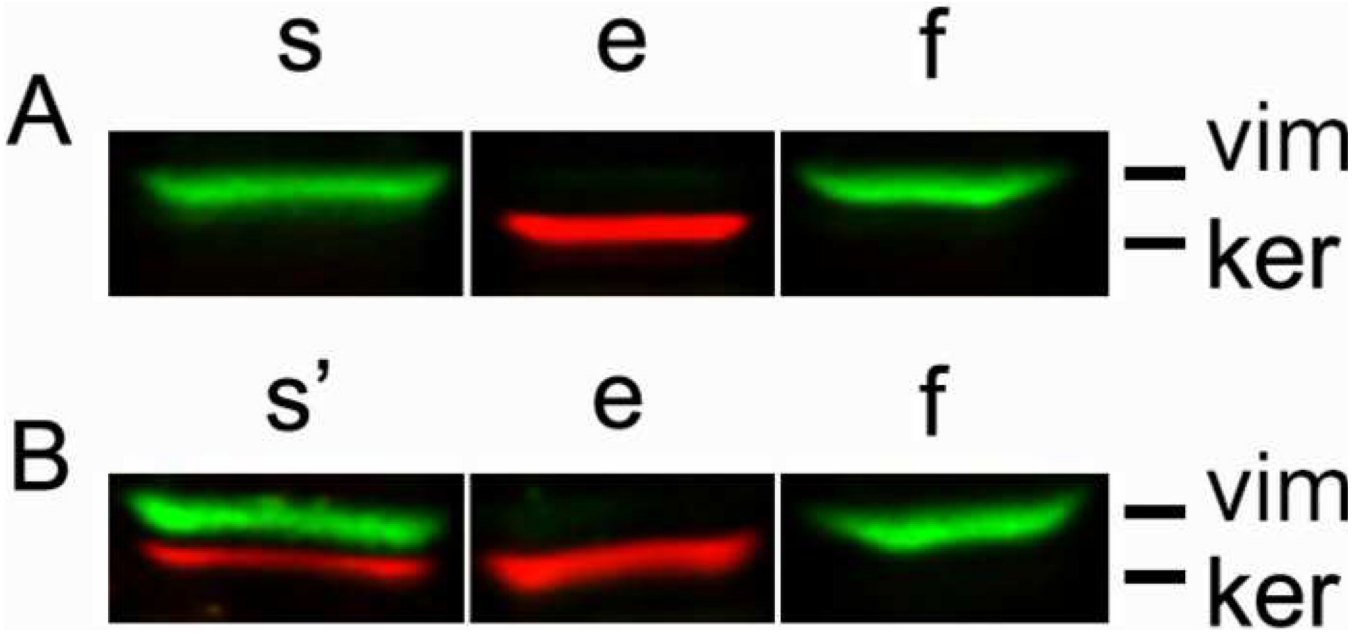

Figure 2. Positive identification of human ovarian fibroblasts

Primary fibroblasts, harvested from fresh ovarian tissue samples (see Materials and Methods), were subjected to Western blot analyses. Cell lysates obtained from epithelial (**e**) and fibroblastic (**f**) cells were compared to sample (**s** and **s**') cells in question. Antibodies against vimentin (**vim**), shown in green, and pan keratin (**ker**), shown in red, were used to probe each sample and identify cell types as fibroblastic or epithelial, respectively. Cells expressing vimentin but not keratin (**A**) were selected for further characterization while double vimentin/keratin positive cells (**B**) were not used in this study. See Materials and Methods for additional details.

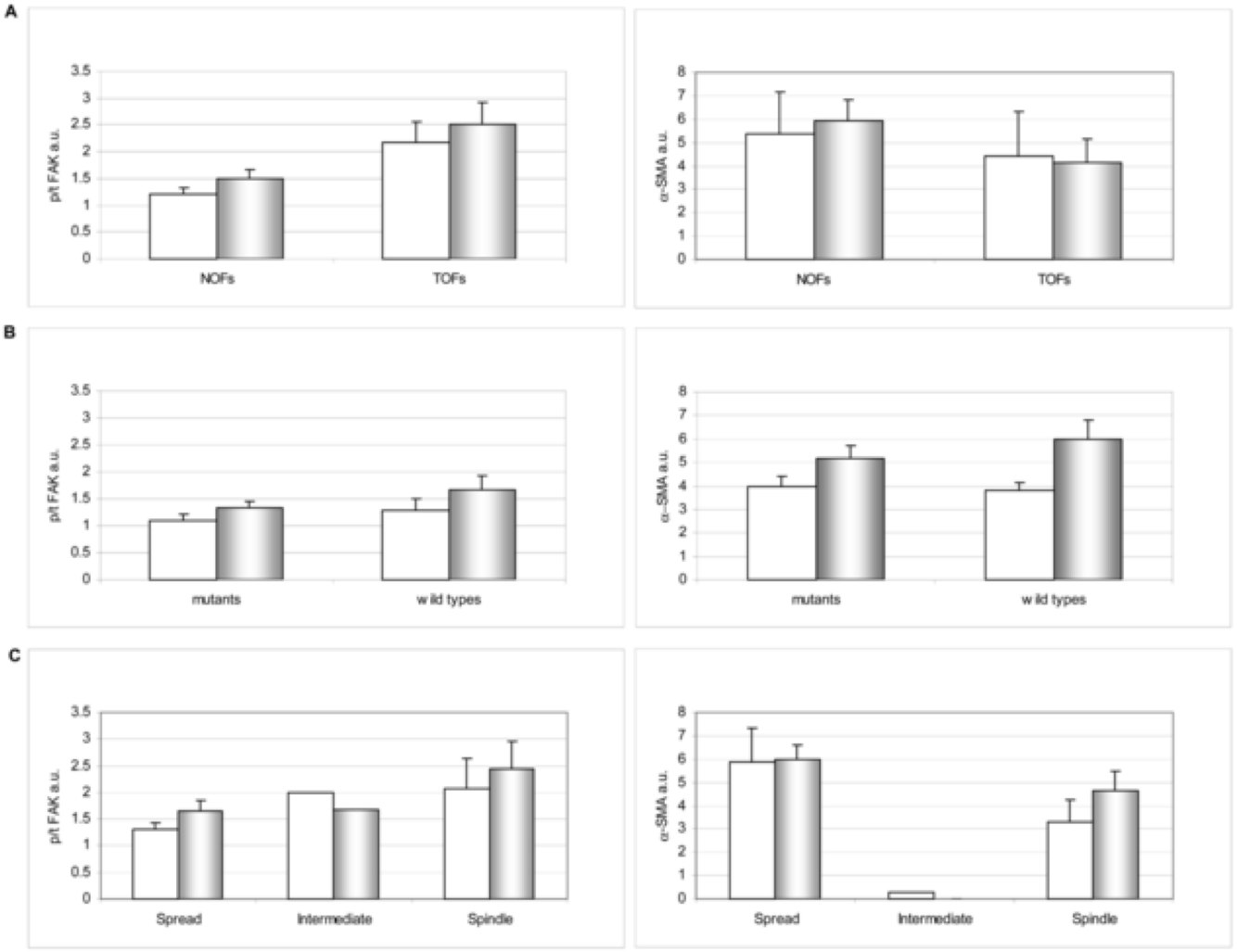

Figure 3. Biochemical characteristics of primary ovarian fibroblastic cells

Cell lysates from 2-D (white bars) and unextracted 3-D cultures (shaded bars) were subjected to Western blot analyses (see Materials and Methods). Levels of total (tFAK) and activated pFAKY^{397} (pFAK), as well as α-SMA expression normalized to GAPDH, were calculated by fluorescent intensity measurements using the Licor Odyssey apparatus and its analysis software. Bar graphs depict specific FAK activities (**p/t FAK**) and **α-SMA** expression levels (normalized to GAPDH levels) of primary ovarian fibroblasts comparing NOFs vs. TOFs (**A**), mutant vs. wild type NOFs (**B**), or all fibroblasts sorted by their morphological 2-D features as spread, intermediate or spindle (**C**). Note that the main observed differences are in panel **C**, where 'spread' and 'spindle' cells present clear FAK activity and even more α-SMA expression differences when compared with intermediate.

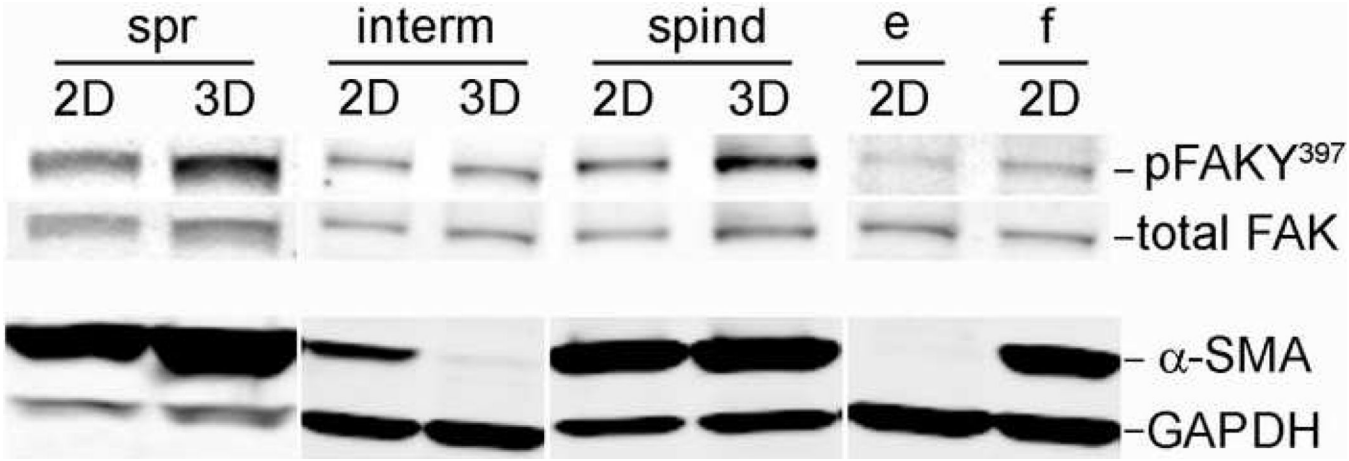

Figure 4. Cells characterized by their 2D morphology as 'spread' and 'spindle' differ in their specific FAK activity and α-SMA expression from 'intermediate' TOFs

2-D and unextracted **3-D** lysates of primary fibroblastic cells, originally sorted as spread (**spr**), intermediate (**interm**) and spindle (**spind**), were subjected to Western blot analyses while 2-D cultures of fibroblastic WI38 (**f**) and epithelial MCF7 (**e**) cells were used as controls. All lysates were probed using antibodies against activated (**pFAKY**^{397}) and total **FAK** or **α-SMA** and **GAPDH** followed by secondary fluorophore-labeled antibodies (see materials and Methods). Images were acquired using the Odyssey apparatus from Licor. Representative monochromic images are shown. Note that while spread and spindle cells show an increase in FAK activity when comparing 2-D vs. 3-D cultures, intermediate cells appear to down regulate both FAK activity and α-SMA expression in a 3-D dependent manner (see Table 2 for complementary data).

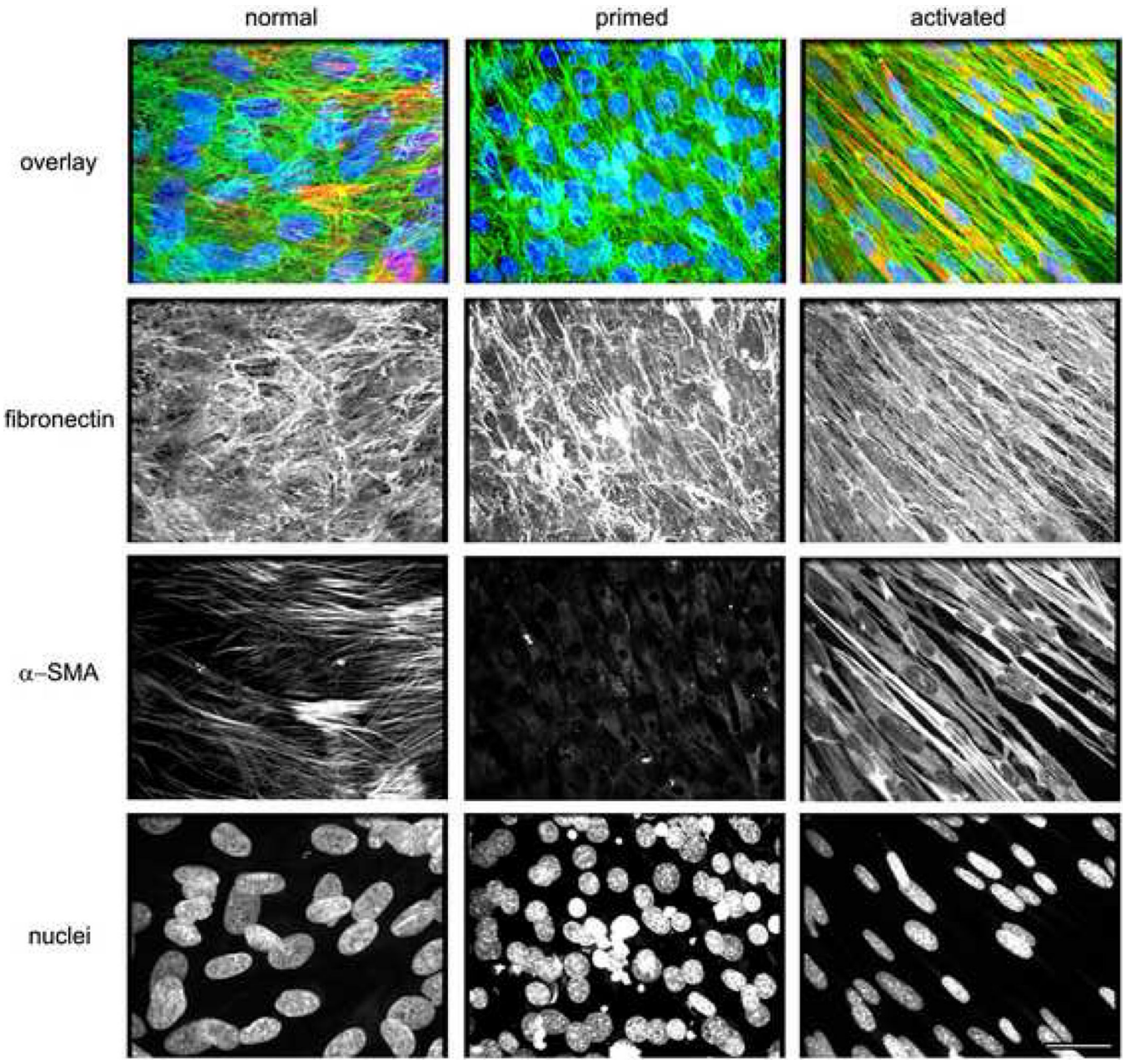

Figure 5. Unextracted 3-D cultures of primary ovarian fibroblasts can be sorted as 'normal,' 'primed' and 'activated.'

Confocal images of indirect immunofluorescently labeled fibronectin rich ECM (in green), α-SMA (in red) and cell-nuclei (in blue) from assorted '**normal**,' '**primed**' and '**activated**' unextracted human primary ovarian fibroblastic 3-D cultures. Top row depicts overlays showing the triple color combinations while bottom rows show the separated monochromatic (black and white) respective images. Note, that 'normal' and 'primed' cultures exhibit similar matrix (**fibronectin**) and **nuclei** characteristics while they differ in **α-SMA** expression levels and localization patterns. Activated fibroblasts present myofibroblastic characteristics such as parallel patterned fibronectin fibers, homogenous α-SMA expression and dense elliptical nuclei. Scale bar represents 15 μm.

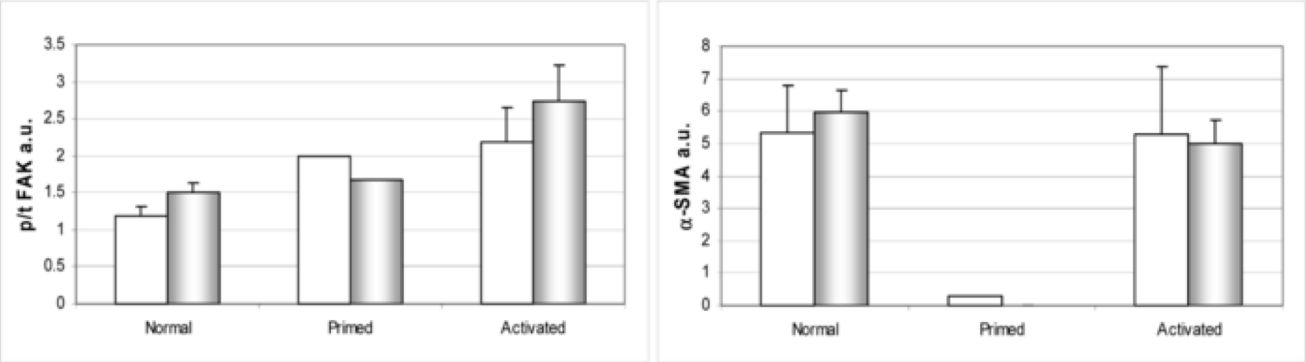

Figure 6. Biochemical characteristics of primary ovarian fibroblasts sorted by stromal stages 'normal,' 'primed' and 'activated.'

Cell lysates from 2-D (white bars) and unextracted 3-D cultures (shaded bars) were subjected to Western blot analyses (see Materials and Methods). Levels of total (tFAK) and activated pFAKY^{397} (pFAK), as well as α-SMA expression normalized to GAPDH, were calculated by fluorescent intensity measurements using the Licor Odyssey apparatus and its analysis software. Graphs depict specific FAK activities (left panel **p/t FAK**) and **α-SMA** (right panel) expression levels of primary ovarian fibroblasts comparing cells sorted, by immunofluorescent analyses of the 3-D cultures (see Figure 5) as '**normal**', '**primed**' or '**activated**.' Note that this biochemical analyses clearly separate '**primed**' from both '**normal**' and '**activated**' fibroblasts.

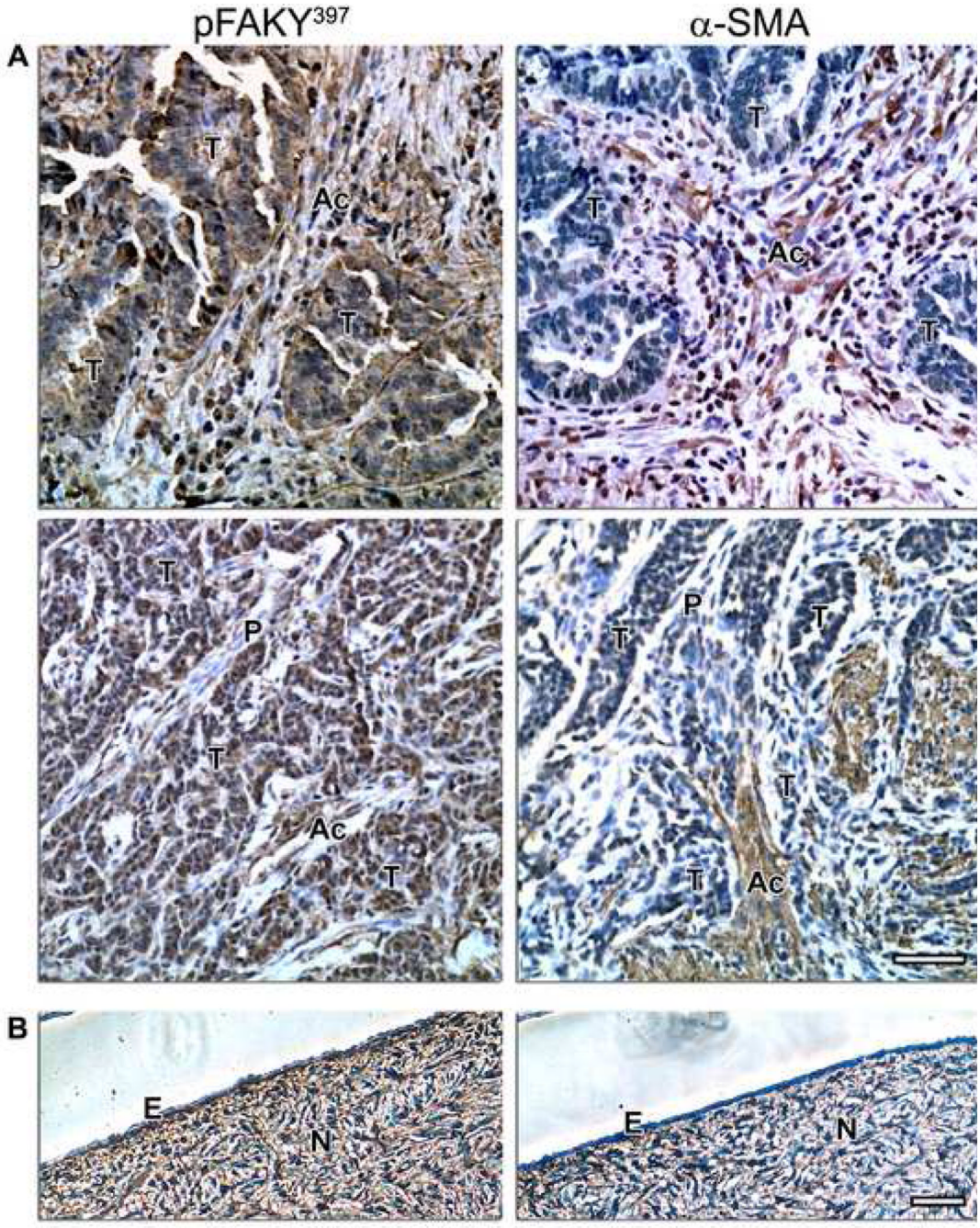

Figure 7. Ovarian 'normal,' 'primed' and 'activated' phenotypes *in vivo* are reminiscent of *in vitro* unextracted 3-D cultures

Immunohistochemistry showing activated FAK (**pFAKY**^{397}) and **α-SMA** levels, counterstained with Harris hematoxylin nucleic stain, of representative cancerous (**A**) and normal (**B**) human ovarian tissues. Normal epithelium (**E**) and tumor areas (**T**), as well as normal (**N**), primed (**P**) and activated (**Ac**) stroma are marked. Note the correlation of pFAKY^{397} and α-SMA in normal and tumor-associated (e.g., activated) stroma in comparison to primed stromal tissue. Scale bars represent, 50 μm.

Table 1

List of human ovarian tissue samples and their harvested cell lines.

Sample	Histopathology	BRCA1 BRCA2 mutation status	Total lines yielded	Morphology in 2D cultures		
				spread	intermediate	spindle
1	Endometrioid adenocarcinoma	ND	3	0	0	3
2	Sex-cord stromal tumor	ND	13	12	1	0
3	Serous adenocarcinoma	ND	9	9	0	0
4	Mucinous cyst-adenocarcinoma	ND	3	3	0	0
5	Clear cell adenocarcinoma	ND	1	1	0	0
6	Normal ovary	1	1	1	0	0
7	Normal ovary	1	1	1	0	0
8	Normal ovary	1	1	1	0	0
9	Normal ovary	WT	1	1	0	0
10	Normal ovary	WT	1	1	0	0
11	Normal ovary	WT	1	1	0	0
12	Normal ovary	1	1	1	0	0
13	Normal ovary	2	1	1	0	0
14	Normal ovary	2	1	1	0	0
15	Normal ovary	1	1	1	0	0
16	Normal ovary	WT	1	1	0	0
17	Normal ovary	WT	1	1	0	0
18	Normal ovary	2	1	1	0	0
19	Normal ovary	1	1	1	0	0
20	Normal ovary	WT	1	1	0	0

Fresh human ovarian **samples** were obtained and numbered as shown in the Table. **Mutation statuses** and **histopathology** information for the samples is provided. Total number of harvested cell lines per sample is listed under '**lines yielded**'. Further sorting according to their morphology in 2-D cultures is reported under '**spread**,' '**intermediate**' or '**spindle**' categories. (WT), patient tested negative for mutations in both BRCA1 and BRCA2, (1), BRCA1 germline mutation carriers, (2), BRCA2 germline mutation carriers, and (ND), not determined. Note that while all normal ovarian samples (6-20) yielded spread morphologies, tumor samples (1-5) yielded more than one morphologic cell type, and sample '2' yielded the only cell line with intermediate morphology. Cultures identified as fibroblastic cells from samples 1-3 and 5-20 and their derived 3-D matrices were submitted to further analyses.

Table 2

FAK specific activity and α-SMA expression in 2-D vs. unextracted 3-D cultures

Sample	p/t FAK (a.u)		α-SMA (a.u)		morphology	stromal stage
	2-D	3-D	2-D	3-D		
1a	3.510688	3.664565	4.768442	2.729572	spindle	activated
1b	2.493075	2.923932	4.991308	4.143342	spindle	activated
2a	1.991342	1.670815	0.302325	0.007041	intermediate	primed
2b	2.655383	3.874818	13.1047	6.310094	spread	activated
3a	1.235808	1.583466	1.389722	6.559197	spread	activated
3b	1.040733	1.609456	2.094714	5.197083	spread	activated
6	1.005451	1.533515	1.749649	4.157934	spread	normal
7	1.16743	1.23406	4.872103	8.763213	spread	normal
8	0.812585	1.18693	4.545376	5.863946	spread	normal
9	1.591667	2.417152	2.919157	7.692373	spread	normal
10	1.769155	1.774064	3.770505	5.069575	spread	normal
11	0.904286	1.147919	3.750612	3.971865	spread	normal
12	2.028826	0.769688	3.954337	3.140526	spread	normal
13	0.835571	1.263254	6.398126	4.574251	spread	normal
14	1.217967	1.790383	4.359564	5.316091	spread	normal
15	1.04019	1.132696	3.144739	6.811327	spread	normal
17	0.887134	1.345262	4.734823	7.2462	spread	normal
18	0.818529	1.070927	3.236699	3.862374	spread	normal
19	0.854295	2.008929	3.645509	3.860075	spread	normal
20	1.831502	2.31746	23.7383	12.90775	spread	normal

Cell lysates from **2-D** and unextracted **3-D** cultures were subjected to Western blot analyses (see Materials and Methods). Specific FAK activities (**p/t FAK**) and levels of **α-SMA**/GPADH expression were obtained by fluorescent intensity measurements using the Licor Odyssey apparatus and its analysis software (see Materials and Methods). Samples were normalized, arbitrary unit=1 (a.u), to the activities and levels obtained from control 2-D fibroblastic (WI38) cultures. Shaded areas depict cell lines harvested from cancerous as opposed to normal ovaries. Corresponding 2-D cultured cell **morphologies** and final sorting of corresponding **stromal-stage** are provided.

Table 3

Sorting characteristics of human ovarian stromal stages; ‘normal,’ ‘primed’ and ‘activated.’

stromal stage	sample number	Results			
		in vitro			*in vivo*
		morphology	WB	IF	IHC
activated	1a	spindle	Highest FAK expression. FAK activity higher in 3-D. Lower than ‘normal’ α-SMA yet similar in 2-D and 3-D.	Myofibroblastic elliptical nuclei and homogenous stress fiber-like α-SMA expression organized in signature matching parallel ECM fibrous patterns.	α-SMA and active FAK in desmoplastic stroma showing typical myofibroblastic string-like features.
	1b	spindle			
	2b	spread			
	3a	spread			
	3b	spread			
primed	2a	intermediate	FAK activity low in 3-D. Lowest α-SMA; decreasing even more in 3-D.	Round nuclei, low α-SMA and disorganized ECM.	Low α-SMA correlates with low active FAK in stroma.
normal	6-20	spread	Lowest FAK with higher activity in 3-D. Highest α-SMA with 3-D increase.	Round nuclei, heterogeneous stress fiber-like α-SMA and disorganized ECM.	Normal postmenopausal stroma expresses α-SMA and some FAK activity.

Summary of observations describing three stromal stages (**activated**, **primed** and **normal**). The table lists the assorted cell number designations (**sample number**), their observed *in vitro* 2-D **morphology**, Western blot analyses (**WB**) of 2-D and 3-D cultures, indirect immunofluorescence (**IF**) of unextracted 3-D cultures and corresponding *in vivo* characteristics of immunohistochemical staining (**IHC**) of representative human ovarian cancerous and normal tissues.